CHAPTER 6. EVALUATION OF CARDIOTHERMAL MODEL PREDICTION OF SIMULATED LUNAR EXTRAVEHICULAR ACTIVITY

6.1 Summary

Fewer than 20 extravehicular activities were completed during the Apollo program. The lunar environment has consistent unknowns to address particularly that of suited performance in partial gravity. The moon has altered gravity that is $1/6^{th}$ that of Earth's. This study is focused to investigate validation of the regression techniques identified in subsequent chapters and look to improve predictive outcomes during simulated lunar EVA tasks. Heart rate predictions of metabolic energy expenditure are investigated from Chapter 5 to predict workload throughout simulated lunar EVA conducted in the active response gravity offload system (ARGOS) within the NASA Mark III space suit. Heart rate variability metrics developed from Chapter 3 are utilized to identify periods of high workload. Continually, the lunar offload capacity is further characterized to aid in improving the cardiothermal prediction models including predictions of core temperature, skin temperature and heat storage using heart rate, metabolic rates and suit thermal data during the simulated EVA. The outcome of this model provides an application for future use in contingency predictions of energy expenditure during Lunar EVAs and provide a suite of instrumentation to predict workload during training scenarios.

6.2 Background

Spaceflight is a limited environment with less than 600 people who have currently been to space and of those only 12 people have walked on the moon. Due to this limited availability, many analogs have been developed to test capabilities for exploration. Most of these analogs focus on low Earth orbit (LEO) for training and suited operations in microgravity [87], [88], [171], [214], [215]. However, as NASA and other space agencies prepare for exploration missions beyond LEO (e.g., the moon and Mars), there are immediate needs to establish ground-based high-fidelity

facilities to support simulated partial-gravity operations. While there is no replacement for the partial gravity effects of spaceflight, NASA has developed several simulation environments, such as, the Partial-Gravity Simulator (POGO), Neutral Buoyancy Laboratory (NBL), parabolic flights and the active response gravity offload system (ARGOS) [216], [217]. Each of these simulation environments have limitations such as work volume, method to reduce gravity offloading and degrees of freedom. The POGO directly impacted participant task performance by only allowing (DOF) in the Y and Z axis while also creating significant overhead inertia and passive horizontal translation [218]. Parabolic flight environment allows for more DOF while providing offloading, though the work volume and duration are limitations (30 seconds per parabola) [219]. The NBL provides a large working volume incorporating International Space Station (ISS) mockup training while allowing full DOF. However, water drag is present effecting the participant during translation and movements [220].

Lastly, the ARGOS provides translational DOF in the horizontal X, Y axis and vertical Z axis (Figure 6.1). In addition to the full DOF the ARGOS also provides robotic active control of offloading, while also providing active control of translational axes movements removing the inertial effects of the system. The ARGOS uses a gimbal design to attach to the human or suit. Specifically, the active robotic components provide three translational DOF and the passive gimble designs provide three rotational DOF. Two different gimbal designs have been used, both have the ability to attach to the NASA Mark III (MK III) waist-ring interface and have customized adjustable center of gravity alignments for the operator [221], [222]. NASA's JSC Human Performance, Physiology, Protection, and Operations (H-3PO) laboratory have used ARGOS to conduct a characterization of EVA metabolic rates simulating planetary exploration-class operations using spacesuit prototypes such as the MK III. [216]

The MK III is a planetary spacesuit assembly used to further assess EVA planetary exploration operations, such as, simulated lunar gravity (Figure 6.1). Historically, Lunar EVA exploration capabilities were tested Apollo A7L. The bioinformatics and portable life support systems (PLSS) for the A7L were designed from previous observations learned from earlier Gemini missions. Specifically, metabolic rates were collected using three different techniques, such as, differential pressure of the PLSS oxygen, heart rate estimations and heat balance of the liquid cooling garment (LCG). The Apollo missions were a huge success but there is room for improvement for future exploration suited operations.

Figure 6.1: NASA MK III within the ARGOS simulated EVA environment.

The MK III has been developed and utilized to evaluate technologies that can further extend planetary EVA capabilities beyond that of the A7L. One large change of the MK III prototype spacesuit compared to other spacesuits is the rear-entry donning/doffing capability. The MK III is

also designed utilizing both hard and soft components. Main elements of the MK III prototype consist of a hard upper torso (HUT), rolling convolute shoulder design, brief and hip translation components, hip and waste abduction/adduction joints, and bearings incorporated in the upper arm, shoulder, hip, ankle and waist [223]–[225]. Also, the MK III neck ring allows for the coupling of a circular removable 13-inch helmet. The suit operates at a nominal 4.3 psig pressure allowing for gas flow rates of 6 ACFM. Breathing gas enters at the rear of the suit helmet via an inlet vent then the gas flows over the top of the head and over the front of the face for CO2 washout. Then the gas flows throughout the body and exits out the suit through an outlet at the lower back plate of the MK III. Main cooling of the suit operator is through a liquid cooling garment (LCG).

While, the MK III and ARGOS provide an environment to test partial-gravity EVA operations there are still unknowns as to how this simulated gravity offloading effects energy expenditure, cardiovascular workload and thermal strain within the suit. One of the limitations to monitor these objective measures is biomedical informatics and instrumentation. The first limitation is focused on the space suit, the limited space within the space suit and around the ARGOS gimble attachment leads to limited availability for space of instrumentation. This study identifies instrumentation to measure thermal loading of space suit operators within the MK III and ARGOS simulated EVAs, then drawing upon previous chapters correlated cardiovascular metrics and metabolic activity metrics are identified to help in predicting accurate physiologic responses to increasing workload. The correlations and predictive models aid in helping reduce the amount of instrumentation needed during training environments increasing fidelity during spaceflight EVA training.

6.3 Methodology

6.3.1 Simulated Gravity Environment and MK III Space suit

The Active Response Gravity Offload System (ARGOS) was used to simulate the effects of offloading during data collection of a Lunar Metabolic Rate Characterization study. Within the simulated environment suit operators donned the rear-entry MK III space suit and were offloaded $1/6^{th}$ G offloading. Metabolic rate during the study was collected through CO2 calculated using a sensor (Vaisala GMP252) in the exhaust stream of the MK III suit REFERENCE. Heart rate for the study is collected from an H-10 Polar heart rate monitor. These measurements were collected every one second recorded via Raspberry PI 3B+. The above mentioned Lunar Metabolic Rate Characterization study was approved by the NASA Johnson Space Center IRB office as not human subject research as part of Human Health and Performance in Spacesuits During Exploration Task Simulations. Two suit operator (S1 and S2) performed two separate ARGOS simulations called Run 1 (R1) and Run 2 (R2) lasting three to five hours performing various metabolically demanding tasks. These tasks included EVA walkback to simulate walking to and from a lunar crater site. This walkback consisted of different walking grades on a treadmill to simulate going up and down lunar crater terrain. Tasks also included geology sampling, cognitive task loads and object relocation.

6.3.2 Suited Thermal Sensor Suite

A suited thermal sensor suite was developed to collect suited performance and human thermal regulation metrics during ARGOS MK-III testing. The thermal sensors were chosen to measure physiologic data of core temperature and skin temperature. Additionally, sensors were selected to measure suited thermal data including liquid cooling garment inlet and outlet temperature, in-suit gas inlet and outlet temperature as well as in-suit inlet and outlet humidity. Further below is a

description of each sensor selected and the location during ARGOS MK-III testing. The controller for data storage and collection was a Raspberry PI model 3B+ and code that was written for data collection was Python.

6.3.2.1 Skin Temperature

Sensors to measure skin temperature were selected for minimizing space within the MK III. These sensors consisted of iButton DS1923 Hygrochron Temperature and Humidity Sensor. The hygrochron iButton sensor sampling rate was every one minute to conserve battery life. Each of the sensors collected localized temperature and humidity and were positioned directly on the skin underneath the LCG on the lower forearm, upper bicep, leg quadricep, leg calf, mid chest, and upper back secured with medical tape (Figure 6.2). From the six locations across the body, mean skin temperature was calculated from weighted average using the Ramanathan method (Eq 6.1) [226], [227]. The mean skin temperature calculation was used in comparisons of the cardiothermal regression model and METMAN thermal outputs.

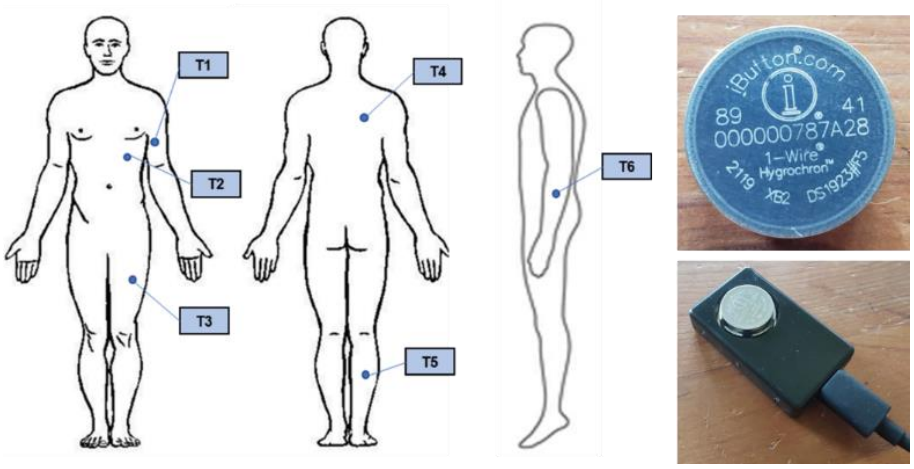

Figure 6.2: Local skin temperature measurements were taken via iButton DS1923 Hygrochron at six locations on the body. Measurements are used to calculated weighted mean skin temperature.

$$\boldsymbol{Ts = 0.3 * (T1 + T2) + 0.2 * (T3 + T5)} \qquad \textbf{Eq. 6.1}$$

6.3.2.2 Core Temperature

Core temperature was collected via the BodyCap eCelsius Performance ingestible pill (Figure 6.3). The pill was ingested three to four hours before the participant donned the MK-III suit and started the EVA. The eCelsius Performance pill transmits in real-time to the eCelsius Viewer by RF transmission (433-434 Hz) and can also store data locally on the pill if connection is lost. The data that is stored is then offloaded onto the eCelsius Viewer upon re-established wireless connection. In this study it was chosen to store the data locally and offload the data after the EVA. The sampling rate was set to 30 seconds to allow for the total amount of data to be stored during the duration of the simulated EVA.

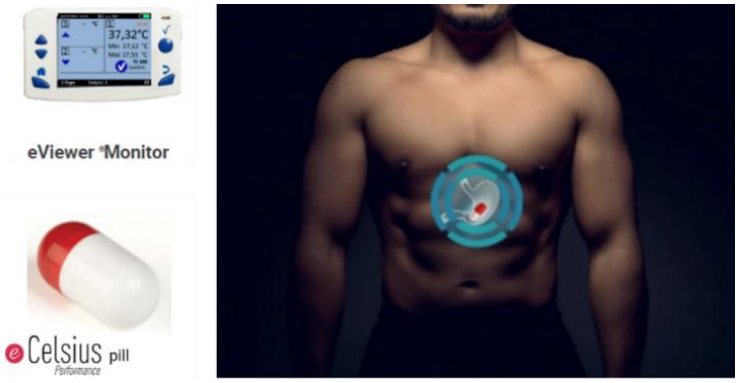

Figure 6.3: Core temperature during the simulated EVA was collected via an ingestible pill three to four hours before the test start to ensure correct location was reached for accurate measurements.

6.3.2.3 Suit LCG Inlet and Outlet Temperatures

LCG inlet temperature provides an input to the human thermal model METMAN for accurate suit thermal regulation. In this study both inlet and outlet temperature were collected to not only provide input into the human thermal model but also to the cardiothermal regression to improve the prediction accuracty of metabolic rate, core temperature and skin temperature. LCG inlet and outlet temperatures were collected via 100 Ohm resistive temperature detectors (RTDs) that were inset into NPT pipe fittings. The RTD was connected to a resistance to digital converter MAX31865 breakout board for input to the Raspberry PI. A pipe fitting tree was designed to

couple between with the ARGOS coolant supply and the MK-III LCG inlet/outlet ports (Figure 6.4). This pipe fitting tree was also designed for quick disconnect to allow removal quickly in case of emergencies. The LCG temperature was sampled every one second and stored on the Raspberry PI.

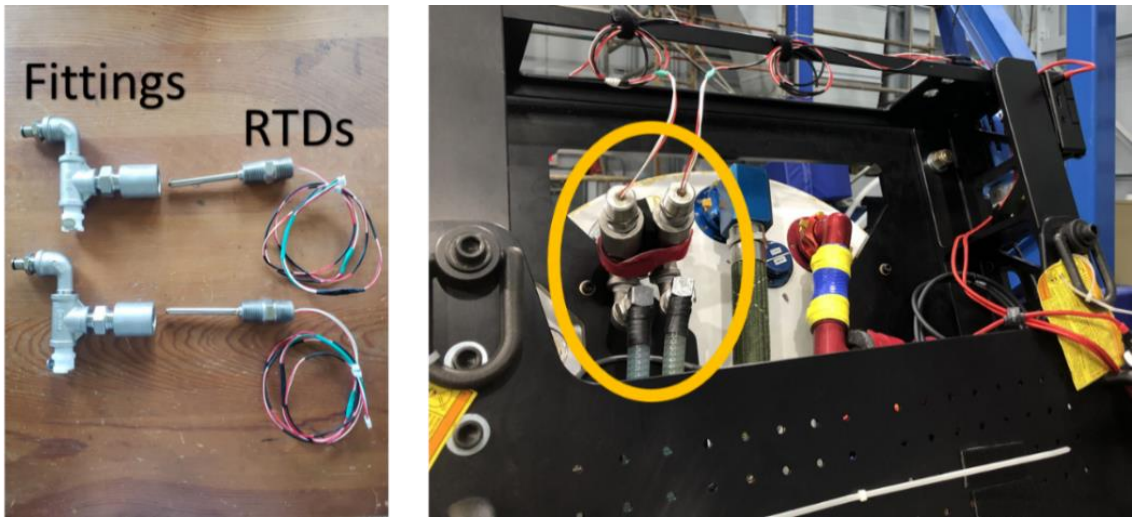

Figure 6.4: Liquid cooling garment inlet and outlet temperatures were gathered via two resistive temperature detectors located in a fittings tree coupled to the back of the MK III.

6.3.2.4 Suit Gas Temperature and Humidity

Similar to LCG inlet temperature, suit gas inlet humidity and temperature are expected inputs to the human thermal model METMAN for accurate thermal regulation characteristics of the suit. In this study the gas inlet and outlet temperatures and humidity are collected for the METMAN model but also to continue to improve the cardiothermal regression model correlations. The inlet suit gas temperature and humidity were collected using the iButton DS1923 Hygrochron Temperature and Humidity sensor located on the inside of the helmet (Figure 6.5). This was chosen due to its small size and location directly inline to the gas flow stream into the helmet for accurate readings. This inlet sensor was collected every one minute to conserve battery life of the iButton Hygrochron. The outlet temperature and humidity were collected via a Vaisala HMP7 Temperature and Humidity sensor located downstream of the suit exhaust. This sensor location is coupled to

the exhaust a Vaisala GMP252 CO2 sensor used to calculate metabolic rate for the study (Figure 6.6). This exact location was chosen to not interfere with the CO2 sensor as the main part of the

Figure 6.5: Suit gas inlet temperature and humidity collected via an iButton Hygrochron positioned at the inlet of the helmet of the MK III.

Lunar Metabolic Rate Characterization study by H-3PO. The Vaisala HMP7 connects to the Raspberry PI via a M12 to RS485 USB and collects by Modbus serial communication. The outlet temperature and humidity are collected every one second with the LCG inlet and outlet temperatures.

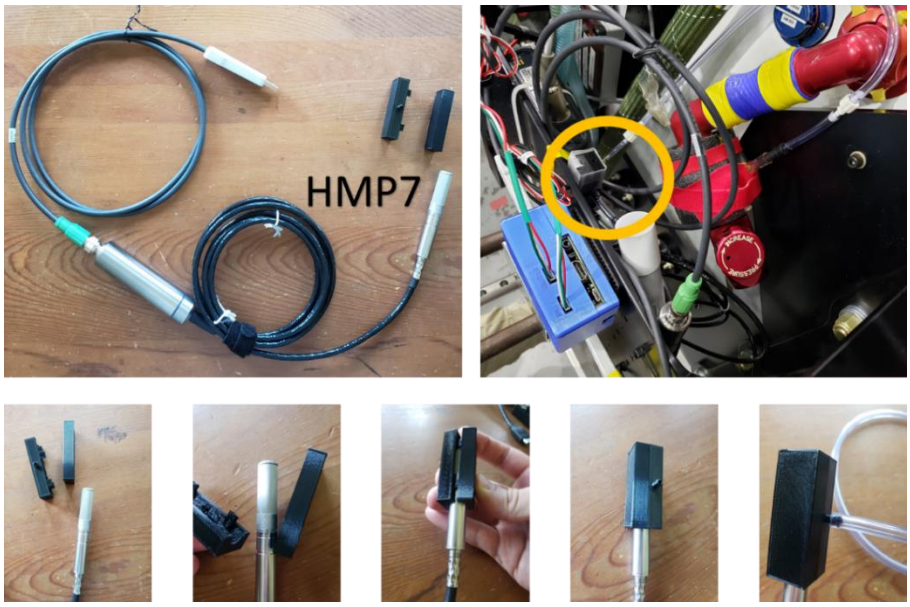

Figure 6.6: Suit gas outlet temperature and humidity is collected using a Vaisala HMP7 temperature and humidity probe located downstream of the exhaust gas of the MK III suit.

6.3.3 Cardiothermal Correlations and Model Evaluation

The first cardiovascular and energy expenditure model tested was utilizing the technique developed from EVA datasets in Chapter 5. Linear regression modeling was fit using Python *statsmodels* regression linear model. An individualized linear regression was built from each subject R1 using metabolic Rate (BTU/hr) as the dependent variable of interest and heart rate as the independent variable. The regression model was then tested in each subject R2 using root mean square error as the determining factor of success from previous Apollo data [207]. Further, the simple metabolic regression model was improved by adding in corresponding MK III suit thermal independent terms creating a multiple regression including LCG inlet temperature, LCG outlet temperature, delta LCG temperature, inlet suit gas temperature, outlet suit gas temperature, delta suit gas temperature, inlet suit humidity, outlet suit humidity, and finally delta suit humidity. Single variable and multivariable models were compared to determine the most linear fit for predicting metabolic rate.

As a continuation the similar technique was used to determine a cardiothermal regression model to predict both core temperature and mean skin temperature during the subject R1 ARGOS simulations. First a simple regression was built for both core temperature and mean skin temperature as the dependent variables and independent terms of heart rate and metabolic rate were used. The regression model was then tested in each subject R2 utilizing root mean square error as the factor for success. The model for core temperature and mean skin temperature regressions were improved for multiple regressions using the same MK III suit terms of LCG temperature, suit gas temperature, and suit humidity. The simple and multiple regression models were compared to determine most linear fit for predicting core temperature and mean skin temperature. Further, the

regression models were compared with outputs from a commonly used human thermal model METMAN.

HRV metrics were collected from the same techniques utilized in Chapter 3 using r-r intervals collected from the polar H-10 and computed using Kubios HRV 3.4.3 for further evaluation and artifact removal. Fast Fourier Transformation (FFT) was used with a 256 s window width and 50% overlap. Time domain features of standard deviation of normal-to-normal sinus beats (SDNN) and root mean square of successive difference (RMSSD) were compiled across R1 and R2 tasks for each suited operator. The low frequency power (LFnu) and high frequency power (HFnu) were calculated from the low frequency band (0.04-0.14 Hz) and the HF band (0.15-0.4 Hz) respectively. The LF/HF ratio was determined from the corresponding values. Additionally, HRV workload status outputs were manually investigated to observe whether high HRV determined workloads corresponded to high metabolic workload and thermal strain (i.e., increased core temperature, modeled heat storage).

6.3.3 Human Thermal Modeling

Considerable work has been conducted by engineers and physiologists to develop and simulate extreme thermal environments through mathematical models. The limited availability and access to these thermal environments (e.g., suited EVA and spaceflight) necessitates continual advancement of simulated human thermal regulation. Particularly with increased movement for planetary exploration operations and long duration spaceflight human thermal regulation during these scenarios will be close to impossible to conduct human based analog testing. Therefore, human thermal models such as METMAN (Metabolic Man), Wissler Model, TAITherm, and Fiala allow physiologic simulated responses to develop equipment requirements to encapsulate extreme contingency scenarios [46], [228]–[232].

Particularly, METMAN and Wissler models incorporate environmental thermal parameters associated with suited thermal dynamics. Used in this study is the 41-node transient metabolic man (METMAN). The model separates the body into ten segments consisting of head, arms, legs, hands, feet and torso. Each segment is further separated into four corresponding inner compartments or nodes consisting of skin, fat, muscle and core (Figure 6.7 A). The last node corresponds to a central blood node. Each compartment is described by mathematical representations of heat transfer between each node with the central blood node representing heat convection through the body segments (Figure 6.7 B).

In this study subject suited MK III thermal data was input into the METMAN model including LCG inlet temperature, in suit gas temperature, in suit gas humidity, external ARGOS

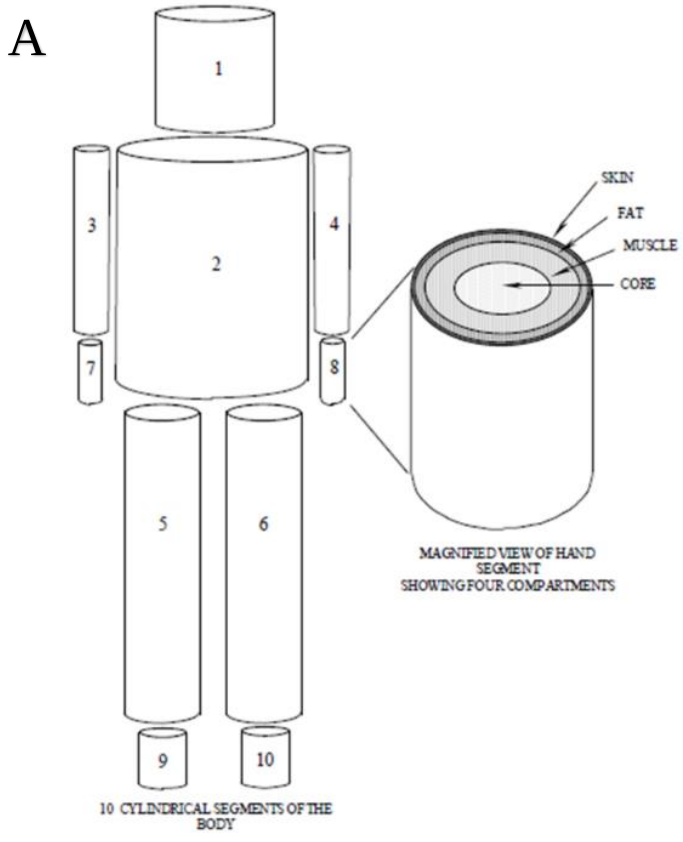

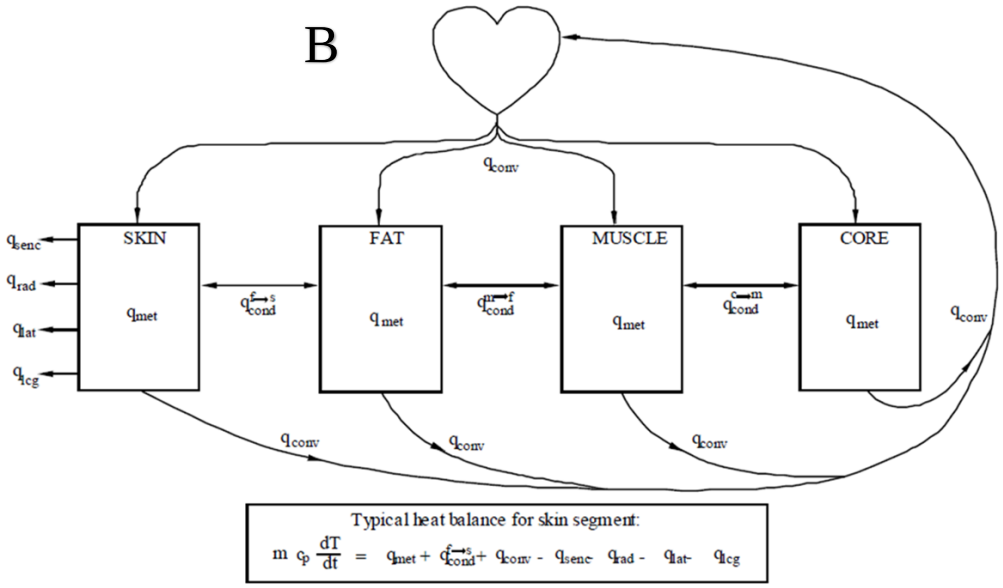

Figure 6.7: Adapted from Bue et al., 41-Node METMAN represented as 10 segments separating head, arms, legs, hands feet and torso further separated into skin, fat, muscle, core (A). Heat balance relation showing heat transfer between segment nodes of skin, fat, muscle and core including convective heat transfer due to blood flow (B).

ambient air temperature and humidity. The inputs are used in the model to build the simulated mathematical representations of the suited environment. Outputs of the model include heat transfer metrics of the suit, such as, LCG heat transfer, suit heat transfer, evaporative, respiration and diffusion heat transfer values. Further, heat storage rate, heat storage total, core temperature, mean skin temperature, heat transfer due to shivering, sweat run off rates, latent heat and evaporative heat transfer are outputs that are used in correlation with collected ARGOS thermal data.

6.4 Results

Metabolic rate predicted from heart rate provided minute by minute evaluation of energy expenditure during simulated EVA. The predicted metabolic rate during the ARGOS simulated lunar EVA was less than the 200 BTU/hr RMSE threshold corresponding to the accuracy of the model technique from Chapter 5 and values determined during Apollo Lunar EVA. The accuracy of the metabolic linear model was improved lowering the RMSE values < 132 BTU/hr and increasing linearity R^2 (> 0.72). This was done by increasing the input of independent terms

through multiple regressions including MK III suit thermal data not previously collected during simulated training. The suited operator values core temperature, heart rate and metabolic rate for each ARGOS simulation can be shown in Table 6.1. Values for core temperature, heart rate and metabolic rates are less during R1 as higher metabolic tasks were planned in R2. Similarly, MK III suited thermal environment values can be found in Table 6.2 for the subsequent ARGOS simulations.

Table 6. 1: Suited Operator Thermal and Cardiovascular Outputs

Operator	Mean Skin Temp (°C)	Core Temp (°C)	Heart Rate (bpm)	Metabolic Rate (BTU/hr)
S1 R1	28.1 ± 1.19	36.7 ± 0.6	56 ± 8	597.4 ± 156.7
S1 R2	27.2 ± 0.69	37.4 ± 0.5	84 ± 17	883.9 ± 364.0
S2 R1	28.5 ± 0.55	37.4 ± 0.3	138 ± 18	859.3 ± 239.5
S2 R2	29.4 ± 1.83	37.6 ± 0.3	143 ± 19	923.46 ± 305.2

Table 6.2: MK III Thermal Environment Outputs

Operator	LCG Inlet Temp (°C)	LCG Outlet Temp (°C)	Suit Inlet Temp (°C)	Suit Outlet Temp (°C)	Suit Inlet Humidity (%)	Suit Outlet Humidity (%)
S1 R1	16.8 ± 2.20	-	23.0 ± 0.62	23.1 ± 0.25	22.5 ± 13.05	21.3 ± 4.48
S1 R2	14.8 ± 0.92	16.9 ± 0.90	22.1 ± 0.30	22.7 ± 0.19	11.1 ± 4.70	24.1 ± 10.50
S2 R1	14.5 ± 0.06	16.4 ± 0.21	22.2 ± 0.20	22.5 ± 0.12	22.7 ± 7.98	28.1 ± 6.52
S2 R2	15.2 ± 1.30	17.2 ± 1.15	22.2 ± 1.18	22.7 ± 0.27	9.9 ± 2.34	28.6 ± 9.65

Significant regression equations were found to predict metabolic rate first with the similar techniques identified in Chapter 5 (Table 6.3). Relationships between metabolic rate from heart rate showed linear trends during R1 with regression responses less than 200 BTU/hr shown in (Figure 6.8A & B). Subsequent significant multiple regressions were found improving the predictive characteristics of the model. The highest accuracy for S1 consisted of heart rate, LCG and suit outlet humidity (RH). LCG parameters for S1 had shown to be less likely to be correlated with metabolic rates while heart rate and outlet humidity showed increased correlations. The model with highest accuracy found for S2, allowed inputs of heart rate, LCG inlet temperature, delta LCG temperature and suit outlet RH (Table 6.3). In comparison to S1, S2 LCG components showed

higher correlations to metabolic rates in the regression model. As a corollary, predicted metabolic rate signals for both S1 and S2 ARGOS simulation during R2 using the multiple regressions showed improved response accuracy, RMSE 175.37 BTU/hr and 177.16 BTU/hr respectively (Figure 6.9A & B).

Table 6.3: Metabolic Rate Regression Model Predictors and Coefficients

PREDICTOR	TEST	COEFFICIENTS	SE	numDf	denDf	T-STAT	PVALUE
S1							
HR^2	Intercept	344.0590	5056	1	10042	67.931	<0.0001
	Slope	0.0756	0.002			44.791	
HR^2+LCG	Intercept	335.9230	10.876	2	10042	30.887	<0.0001
	X1	0.0761	0.002			42.317	<0.0001
	X2	0.3932	0.465			0.845	0.398
HR^2+LCG+RH	Intercept	284.4705	11.466	3	10042	24.809	<0.0001
	X1	0.0748	0.002			41.874	<0.0001
	X2	0.0888	0.462			0.192	0.847
	X3	2.8352	0.215			13.199	<0.0001
S2							
HR^2	Intercept	42.3454	6.674	1	7147	6.344	<0.0001
	Slope	0.0415	< 0.001			128.585	
HR^2+LCG	Intercept	12270	511.797	2	7147	23.971	<0.0001
	X1	0.0452	< 0.001			130.250	
	X2	-849.3019	35.550			-23.891	
HR^2+LCG+ΔLCG	Intecept	18490	674.452	3	7147	27.417	<0.0001
	X1	0.0455	< 0.001			132.652	
	X2	-1215.8689	43.863			-27.720	
	X3	-526.7327	37.837			-13.921	
HR+LCG+ΔLCG+RH	Intercept	16440	755.483	4	7147	21.766	<0.0001
	X1	0.0452	< 0.001			130.706	
	X2	-1070.2644	50.115			-21.356	
	X3	-475.4377	38.715			-12.281	
	X4	-6.2176	1.043			-5.960	

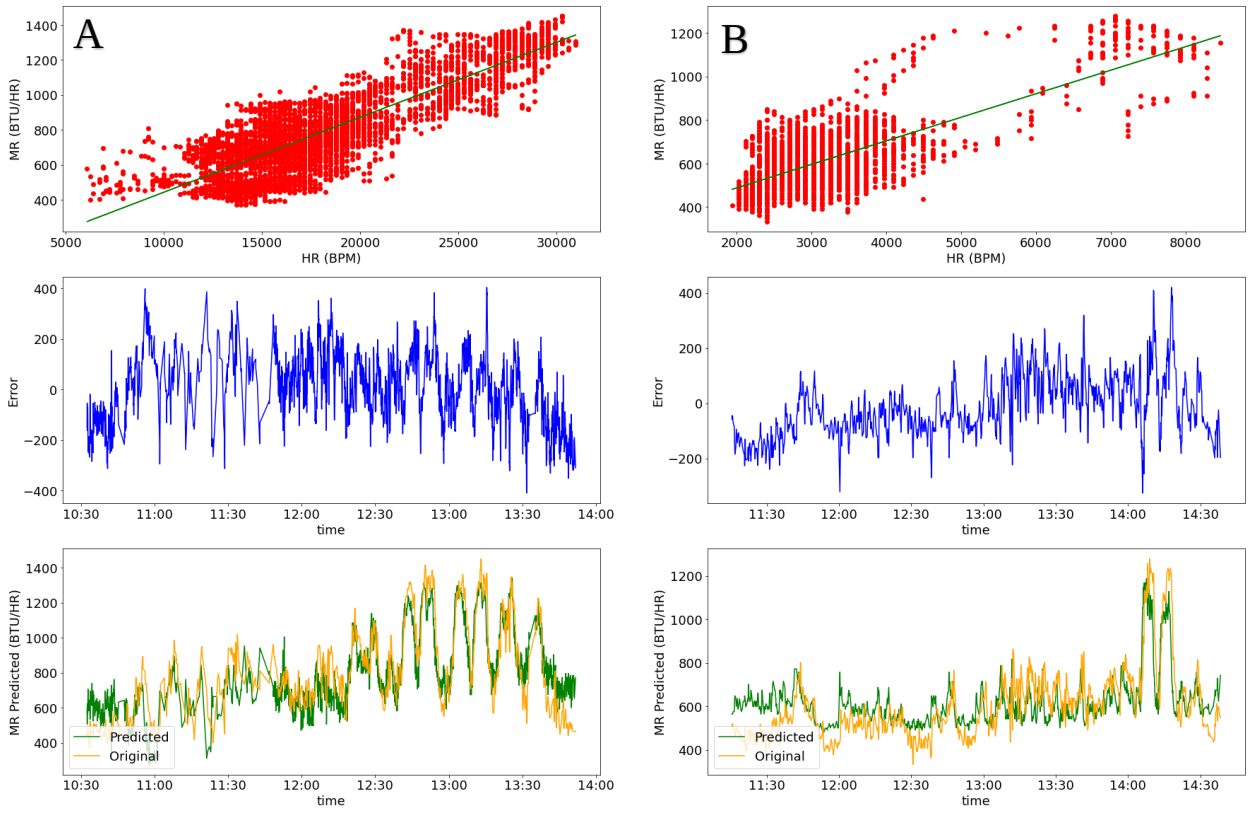

Figure 6.8: Predicted regression responses of the first run for both suited operators. Suited operator one R1 metabolic rate regression built from only heart rate inputs column (A). Suited operator two R1 metabolic regression built from only heart rate inputs column (B). Both responses yield RMSE < 150 BTU/hr.

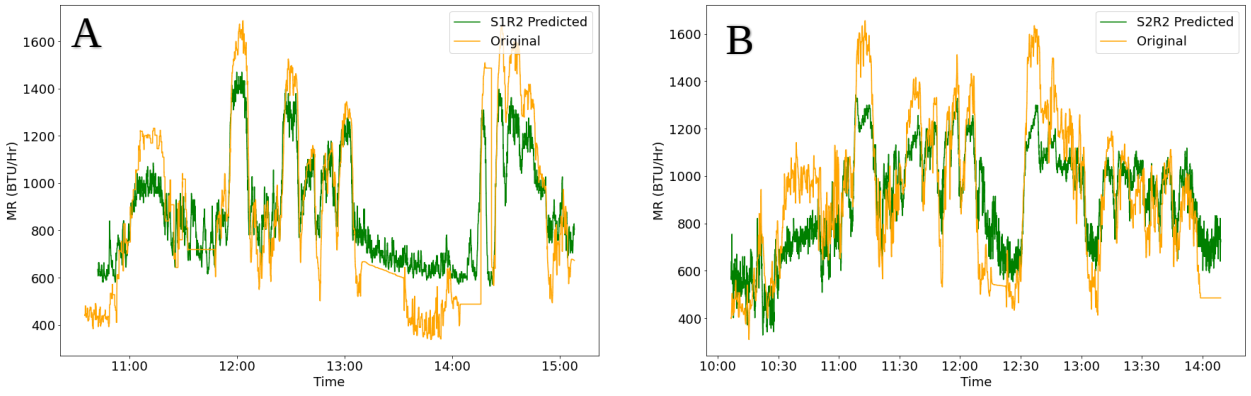

Figure 6.9: ARGOS R2 lunar EVA simulations predicted metabolic rate outputs from regression model for both suit operator S1 (A) and suit operator S2 (B) ARGOS R2 simulations. Both RMSE < 200 BTU/hr.

Predicting core temperature and mean skin temperature was found utilizing the same linear regression observations that were used to determine metabolic rate. It was found that for simple single linear regressions a significant regression equation was found for both heart rate and

metabolic rate as the independent predictors for core temperature and mean skin temperature (Table 6.4, Table 6.5). Additionally, the metric developed in chapter 5 of MR/HR as a BTU/beat showed correlations through a significant regression equation with core temperature. Additionally, delta LCG temperature and suit outlet RH also showed significant regression equations in predicting core temperature. However, LCG inlet temperature alone did not have a high correlation in the predictions of core temperature regressions.

While these regression equations were significant, the accuracy and linearity of the model was lower for the single input models. The core temperature and mean skin temperature linear models were improved by adding multiple regression terms using the highest correlated single terms such as, MK III thermal suited metrics of delta LCG inlet temperature, suit gas outlet RH values, metabolic rate and MR/HR values (Table 6.4, Table 6.5). For S1 the core temperature model with the most accuracy consisted of the terms metabolic rate (MR), MR/HR and outlet RH, RMSE 0.46 C. While for S2 the most accuracy was attained using MR, MR/HR, Δ LCG, and suit outlet RH, RMSE 0.12 C. In comparison, the thermal model METMAN outputs of core temperature showed similar correlations to the regression models. The METMAN output of core temperature for S1 R2 resulted in higher accuracy with RMSE 0.29 C (Figure 6.10 A, Figure 6.11 A). While the S2 core temperature regression model outperformed the METMAN output, RMSE 0.12 and 0.23 C respectively (Table 6.6).

Conversely to core temperature, mean skin temperature had shown more reactive responses to changes in LCG while lowest responses were attributed to HR, MR, and RH values. The highest mean skin temperature regression consisted of values of MR/HR and LCG inlet for S1 RMSE 0.67 C and MR/HR, LCG and Δ LCG for S2, RMSE 0.74 C. The regression model for mean skin temperature outperformed the METMAN predicted mean skin temperature (Table 6.6). Values in

comparison for mean skin temperature were S1 (0.67 C) and S2 (0.74 C) compared to METMAN mean skin temp RMSE 1.02 C and 1.12 C respectively (Figure 6.10 B, Figure 6.11 B).

Table 6. 4: Core Temp Regression Model Predictors and Coefficients

PREDICTOR	TEST	COEFFICIENTS	SE	numDf	denDf	T-Stat	PVALUE
S1							
HR	Intercept	37.3254	0.245	1	210	152.239	< 0.0001
	Slope	-0.0110	0.005			-2.397	0.017
MR	Intercept	37.6897	0.112	1	210	335.885	< 0.0001
	Slope	-0.0016	< 0.001			-8.590	
MR/HR	Intercept	37.6799	0.125	1	210	302.553	<0.0001
	Slope	-0.0858	0.011			-7.643	
LCG	Intercept	36.5797	0.174	1	210	210.144	< 0.0001
	Slope	0.0093	0.010			0.929	0.354
Suit Outlet RH	Intercept	36.4892	0.097	1	210	377.635	< 0.0001
	Slope	0.0116	0.004			2.669	0.008
MR+MR/HR+RH	Intercept	37.4842	0.143	3	210	262.291	< 0.0001
	X1	-0.0013	< 0.001			-3.515	
	X2	-0.0223	0.021			-1.052	
	X3	0.0118	0.004			3.159	
S2							
HR	Intercept	36.7886	0.122	1	303	301.553	< 0.0001
	Slope	0.0042	0.001			4.715	
MR	Intercept	37.3873	0.062	1	303	600.442	< 0.0001
	Slope	-0.00003	<0.001			-0.472	0.637
MR/HR	Intercept	37.7094	0.085	1	303	445.873	<0.0001
	Slope	-0.0572	0.014			-4.221	
LCG	Intercept	2.6477	3.767	1	303	0.703	0.483
	Slope	2.3900	0.259			9.214	< 0.0001
Δ LCG	Intercept	34.9333	0.106	1	303	330.843	< 0.0001
	Slope	1.2986	0.056			23.074	
Suit Outlet RH	Intercept	36.1141	0.060	1	303	605.313	< 0.0001
	Slope	0.0489	0.002			21.192	
MR+MR/HR+ΔLCG	Intercept	34.8380	0.107	3	303	324.745	< 0.0001
	X1	0.0042	0.001			4.865	
	X2	-0.0004	< 0.001			-6.751	
	X3	1.2352	0.057			21.592	
MR+MR/HR+ +ΔLCG+RH	Intercept	35.1998	0.103	4	303	340.818	< 0.0001
	X1	0.0001	< 0.001			1.874	0.062
	X2	-0.0396	0.014			-2.840	< 0.0001
	X3	0.8563	0.056			15.163	< 0.0001
	X4	0.0272	0.002			12.095	< 0.0001

Table 6.5: Mean Skin Temperature Regression Model Predictors and Coefficients

PREDICTOR	TEST	COEFFICIENTS	SE	numDf	denDf	T-Stat	PVALUE
S1							
HR	Intercept	27.8335	0.577	1	151	48.219	< 0.0001
	Slope	0.0122	0.010			1.210	0.228
MR	Intercept	28.0063	0.345	1	151	81.281	< 0.0001
	Slope	0.0008	0.001			1.554	0.122
MR/HR	Intercept	27.7478	0.525	1	151	52.898	< 0.0001
	Slope	0.0698	0.047			1.501	0.136
LCG	Intercept	22.7698	0.506	1	151	44.987	< 0.0001
	Slope	0.3329	0.029			11.464	
Suit Outlet RH	Intercept	28.3995	0.398	1	151	71.406	< 0.0001
	Slope	0.0058	0.018			0.320	0.749
MR/HR+LCG	Intercept	20.6448	0.658	3	151	31.370	< 0.0001
	X1	0.1520	0.033			4.658	
	X2	0.3581	0.028			12.908	
S2							
HR	Intercept	26.9176	0.336	1	151	80.074	< 0.0001
	Slope	0.011	0.002			4.519	
MR	Intercept	28.1315	0.171	1	151	164.323	< 0.0001
	Slope	0.0003	< 0.001			1.773	0.078
MR/HR	Intercept	28.5896	0.240	1	151	119.305	< 0.0001
	Slope	-0.0273	0.039			-0.704	0.482
LCG	Intercept	-33.1389	10.169	1	151	-3.259	0.001
	Slope	4.2398	0.700			6.054	< 0.0001
Δ LCG	Intercept	23.2180	0.248	1	151	93.711	< 0.0001
	Slope	2.7874	0.132			21.105	
Suit Outlet RH	Intercept	26.5024	0.124	1	151	214.385	< 0.0001
	Slope	0.0685	0.004			15.964	
MR/HR+LCG+ΔLCG	Intercept	25.1136	6.458	3	151	3.889	< 0.0001
	X1	-0.0552	0.019			-2.883	
	X2	-0.1134	0.456			-0.249	
	X3	2.8337	0.153			18.527	

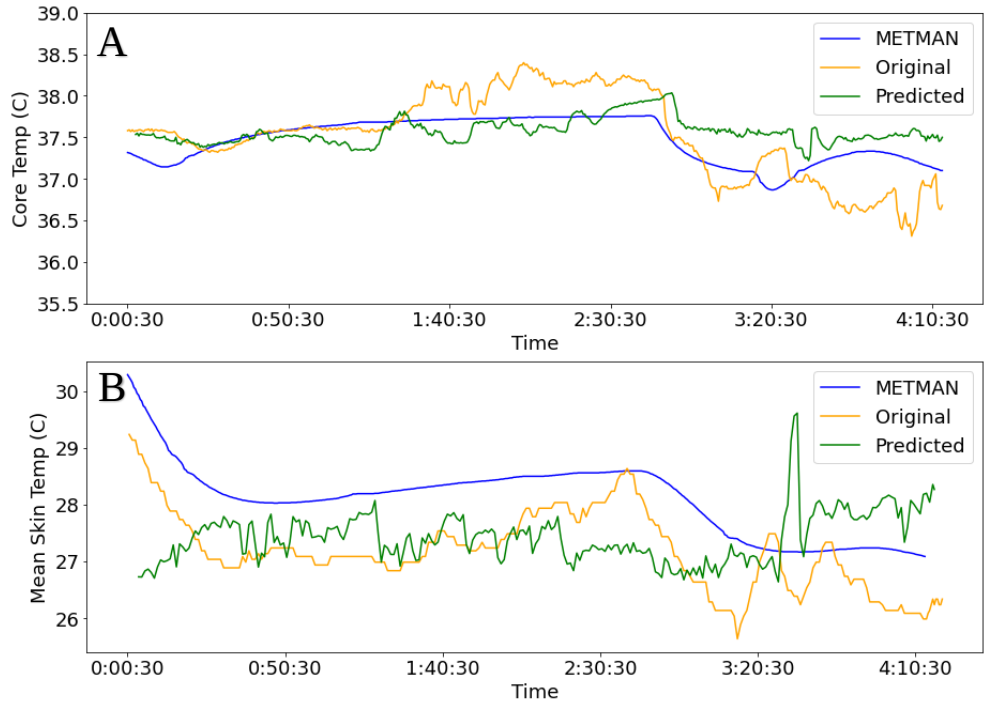

Figure 6.10: Core temperature and mean skin temperature predicted outputs compared to original measured values for S1 ARGOS EVA simulation R2. Core temperature predictions using the multiple regression model of physiologic inputs with suit thermal inputs showed prediction results similar to that of METMAN thermal outputs (A). Mean skin temperature prediction showed that the regression model performed at higher accuracy than METMAN simulated outputs (B).

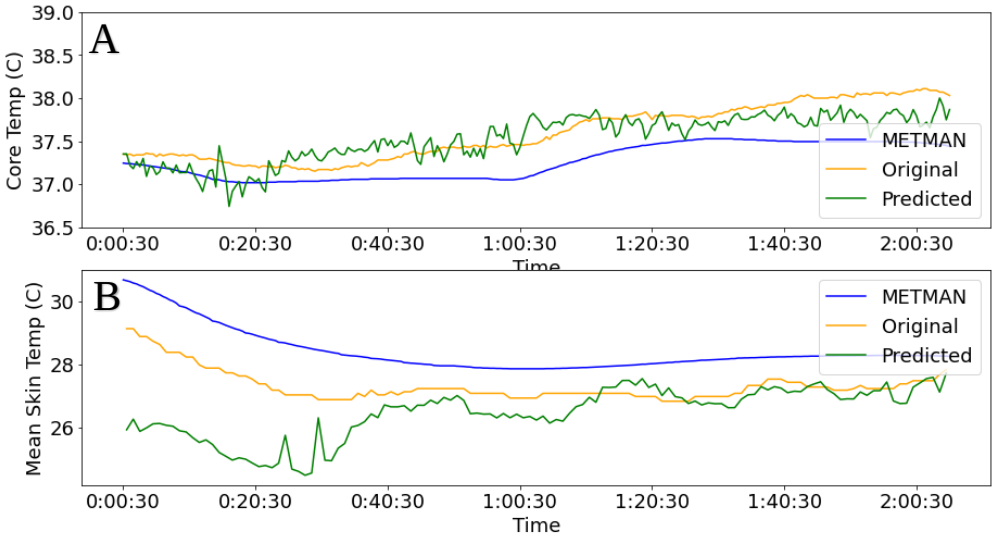

Figure 6. 11: Core temperature and mean skin temperature predicted outputs compared to original measured values for S2 ARGOS EVA simulation R2 first two hours. Core temperature predictions using the multiple regression model of physiologic inputs with suit thermal inputs showed to have better accuracy compared to results of METMAN thermal outputs (A). Mean skin temperature prediction showed that the regression model also performed at higher accuracy than METMAN simulated outputs (B).

Table 6.6: Thermal measured values compared to METMAN and cardiothermal regression predictions.

Operator	Core (°C)	METMAN Core (°C)	METMAN RMSE Core (C)	Regression Core (°C)	Core Temp RMSE (C)	Mean Skin Temp (°C)	METMAN Skin Temp (°C)	METMAN RMSE Skin (C)	Regression Skin Temp (°C)	Skin Temp RMSE (C)
S1 R2	37.5 ± 0.5	37.4 ± 0.3	0.29	37.6 ± 0.2	0.46	27.2 ± 0.7	28.4 ± 0.5	1.02	27.4 ± 0.4	0.67
S2 R2	37.6 ± 0.3	37.3 ± 0.2	0.23	37.5 ± 0.2	0.12	27.4 ± 0.5	29.3 ± 0.4	1.15	26.5 ± 0.7	0.74

HRV metrics of were obtained utilizing the same techniques on Chapter 3. During increased metabolically demanding tasks LF values were shown to increase while HF values were shown to decrease for both S1 and S2 (Table 6.7 and Table 6.8). As a result, LF/HF values were shown to also increase due to metabolically demanding tasks. HF values showed more sensitivity during R2 tasks than LF values compared to R1 simulated EVAs.

Time domain features of RMSSD and SDNN values were higher during tasks with higher metabolic rates and decreased with decreasing metabolic demand (Table 6.9, Table 6.10). This corresponds directly to increased maximum and minimum heart rates during increased metabolic loading. Non-linear metrics of SD1 showed to decrease with lowering metabolic demand while SD2 showed to increase with increasing metabolic rates. The ratio of SD2/SD1 showed to increase with higher metabolic demanding tasks. DFA Alpha-2 had shown to increase with tasks requiring higher metabolic loads (Table 11, Table 12).

Table 6.7: Task based metabolic rates and HRV frequency domain metrics of S1 and S2 R1 simulated EVA.

Task	Metabolic Rate (BTU/hr)		LF (n.u.)		HF (n.u.)		LF/HF	
	S1	S2	S1	S2	S1	S2	S1	S2
Suit Settings	478.54 ± 52.22	679.13 ± 159.36	42.13	56.90	57.86	43.04	0.73	1.32
Primus Movement	660.94 ± 79.55	752.84 ± 101.21	79.31	83.90	20.68	16.07	3.84	5.22
Object Relocation	904.33 ± 246.98	1093.22 ± 227.75	81.65	85.51	18.34	14.46	4.45	5.91
“Rest”	781.34 ± 244.10	539.69 ± 75.75	62.95	71.51	37.03	28.48	1.70	2.511

Table 6.8: Task based metabolic rates and HRV frequency domain metrics of S1 and S2 R2 simulated EVA.

Task	Metabolic Rate (BTU/hr)		LF		HF		LF/HF	
	S1	S2	S1	S2	S1	S2	S1	S2
Up/Down Ladder	732.16 ± 64.92	601.83 ± 62.18	87.86	82.48	12.11	17.49	7.25	4.72
1.5 Km walk	1114.59 ± 130.70	931.72 ± 120.66	78.56	79.93	21.41	20.05	3.67	3.99
Geo 1	798.75 ± 120.93	872.31 ± 130.65	81.65	74.83	18.31	25.15	4.46	2.98
30% 500m	1328.01 ± 311.62	1413.37 ± 239.75	88.94	89.98	11.03	10.09	8.06	8.91
Geo 2	770.20 ± 126.23	879.53 ± 185.04	84.60	60.85	15.38	39.09	5.50	1.56
20% 500m	1203.18 ± 273.13	1201.40 ± 161.52	86.95	85.68	13.02	14.30	6.68	5.99
Obj Relocation	945.88 ± 176.45	1092.32 ± 216.04	71.71	80.47	28.22	19.50	2.54	4.13
10 % Grade 500m	1116.78 ± 183.01	1212.31 ± 183.95	77.28	78.70	22.70	21.24	3.40	3.71
“Rest”	629.63 ± 12.98	564.37 ± 48.09	70.18	72.18	29.76	27.80	2.36	2.60
2 Km walk back	1321.11 ± 271.57	1231.48 ± 242.08	89.92	82.75	10.06	17.19	8.94	4.81

Table 6.9: Task based metabolic rates and HRV Time Domain metrics of S1 and S2 R1 simulated EVA.

Task	Metabolic Rate (BTU/hr)		Mean RR		Max HR		Min HR		RMSSD		SDNN	
	S1	S2	S1	S2	S1	S2	S1	S2	S1	S2	S1	S2
Suit Settings	478.54 ± 52.22	679.13 ± 159.36	1213.0	538.90	75	156	41	62	133.3	56.21	99.33	59.0
Primus Movement	660.94 ± 79.55	752.84 ± 101.21	1197.2	508.16	76	155	41	89	43.61	31.28	51.53	48.78
Object Relocation	904.33 ± 246.98	1093.22 ± 227.75	848.7	397.31	92	170	50	116	25.61	3.81	37.30	7.06
“Rest”	781.34 ± 244.10	539.69 ± 75.75	1085.7	430.82	67	169	48	83	31.06	14.39	30.09	20.22

Table 6.10: Task based metabolic rates and HRV Time Domain metrics of S1 and S2 R2 simulated EVA.

Task	Metabolic Rate (BTU/hr)		Mean RR		Max HR		Min HR		RMSSD		SDNN	
	S1	S2	S1	S2	S1	S2	S1	S2	S1	S2	S1	S2
Up/Down Ladder	732.16 ± 64.92	601.83 ± 62.18	802.03	622.82	91	127	60	64	23.91	43.50	35.86	59.54
1.5 Km walk	1114.59 ± 130.70	931.72 ± 120.66	712.72	488.89	119	136	57	74	22.89	13.87	26.12	18.68
Geo 1	798.75 ± 120.93	872.31 ± 130.65	689.27	479.25	136	142	62	80	17.69	12.49	25.50	19.79
30% 500m	1328.01 ± 311.62	1413.37 ± 239.75	701.81	393.69	109	197	65	97	19.09	8.29	30.94	11.83
Geo 2	770.20 ± 126.23	879.53 ± 185.04	893.25	443.66	80	155	59	89	27.70	7.59	39.18	14.99
20% 500m	1203.18 ± 273.13	1201.40 ± 161.52	945.21	398.05	79	162	55	128	32.60	3.16	48.46	5.83
Object Relocation	945.88 ± 176.45	1092.32 ± 216.04	992.74	380.20	105	168	54	136	40.56	2.15	51.95	4.44
10 % Grade 500m	1116.78 ± 183.01	1212.31 ± 183.95	1002.95	391.66	78	172	52	95	30.66	7.93	38.86	12.03
"Rest"	629.63 ± 12.98	564.37 ± 48.09	778.91	534.92	115	130	50	74	32.76	29.59	31.22	47.31
2 Km walk back	1321.11 ± 271.57	1231.48 ± 242.08	682.66	394.99	113	171	62	82	15.27	6.60	26.13	11.00

Table 6.11: Task based metabolic rates and HRV non-linear metrics of S1 and S2 R1 simulated EVA.

Task	Metabolic Rate (BTU/hr)		SD1		SD2		SD2/SD1		Alpha-1		Alpha-2	
	S1	S2	S1	S2	S1	S2	S1	S2	S1	S2	S1	S2
Suit Settings	478.54 ± 52.22	679.13 ± 159.36	94.85	40.02	140.8	138.80	1.48	3.47	0.91	1.12	0.96	0.86
Primus Movement	660.94 ± 79.55	752.84 ± 101.21	31.75	22.52	182.5	106.53	5.75	4.73	1.40	1.35	1.04	0.91
Object Relocation	904.33 ± 246.98	1093.22 ± 227.75	18.80	2.75	239.3	55.65	12.73	20.24	1.40	1.52	1.25	1.13
"Rest"	781.34 ± 244.10	539.69 ± 75.75	21.56	10.28	21.56	77.08	4.96	7.50	1.32	1.07	1.30	0.92

Table 6.12: Task based metabolic rates and HRV non-linear metrics of S1 and S2 R2 simulated EVA.

Task	Metabolic Rate (BTU/hr)		SD1		SD2		SD2/SD1		Alpha-1		Alpha-2	
	S1	S2	S1	S2	S1	S2	S1	S2	S1	S2	S1	S2
Up/Down Ladder	732.16 ± 64.92	601.83 ± 62.18	17.31	31.14	115.77	131.95	6.69	4.24	1.47	1.34	1.11	0.89
1.5 Km walk	1114.59 ± 130.70	931.72 ± 120.66	16.44	8.97	217.38	52.23	13.22	5.82	1.41	1.43	1.24	0.88
Geo 1	798.75 ± 120.93	872.31 ± 130.65	12.85	9.91	140.46	47.22	10.93	4.76	1.62	1.49	1.27	1.04
30% 500m	1328.01 ± 311.62	1413.37 ± 239.75	13.76	5.99	155.24	54.67	11.28	9.13	1.57	1.51	1.13	0.98
Geo 2	770.20 ± 126.23	879.53 ± 185.04	19.93	5.47	79.21	49.28	3.97	9.00	1.45	1.68	0.92	1.07
20% 500m	1203.18 ± 273.13	1201.40 ± 161.52	23.49	2.28	90.85	28.24	3.87	12.34	1.51	1.63	0.76	1.31
Obj Relocation	945.88 ± 176.45	1092.32 ± 216.04	29.02	1.57	97.98	19.37	3.37	12.30	1.41	1.56	0.94	1.28
10 % Grade 500m	1116.78 ± 183.01	1212.31 ± 183.95	22.12	5.67	111.09	43.73	5.02	7.71	1.43	1.46	1.07	1.20
“Rest”	629.63 ± 12.98	564.37 ± 48.09	23.45	21.25	298.70	76.30	12.74	3.60	1.20	1.39	1.43	0.87
2 Km walk back	1321.11 ± 271.57	1231.48 ± 242.08	11.03	4.74	148.30	42.32	13.45	8.92	1.46	1.52	1.02	1.20

6.5 Discussion

The first objective of this chapter was to determine if the techniques developed in subsequent chapters could predict metabolic and workload rates. Metabolic rates and demand were predicted using a simple linear regression from heart rates for simulated Lunar EVA in the ARGOS. These simple linear regressions were comparable to RMSE error values determined during Apollo Lunar EVAs, the threshold being less than 200 BTU/hr. Utilizing the additional factors of thermal instrumentation on the MK III the metabolic rate regression model accuracy was increased by adding more terms. These thermal suit parameters of inlet LCG temperature, outlet LCG temperature, suit inlet/outlet temperature as well as suit inlet/outlet humidity provided extra environmental factors that attribute to human thermal regulation and ultimately effect metabolic energy expenditure. The final accuracy for suited operator predicted outputs decreased RMSE to

< 180 BTU/hr while also capturing increased R^2 of greater than 0.72. During the S1 R1 simulated EVA the outlet LCG values were not capture due to technical error. As a result, the regression for S1 R2 did not include ΔLCG temperature which caused a slightly higher RMSE compared to the S1 R2 model.

As the general metabolic regression models increases in linearity with increased term inputs, there are still some pitfalls that occur with this technique. The model is only as good as the input values of metabolic rates and thermal parameters. Due to this fact, the regression model does lose resolution when attempting to predict high peak metabolic values greater than 1400 BTU/hr. In turn, the model also loses resolution when predicting absolute minimum values of < 400 BTU/hr (Figure 6.9A and B). However, the heart rate determinations of metabolic energy expenditure can provide an accurate prediction in a minute-by-minute real-time environment. This factor can be improved by incorporating individual crew responses of a range of metabolic activity with correlated cardiovascular function.

The second objective for this chapter was to build upon those techniques to determine thermal loading with the simulated lunar EVA environment. Simulations were completed using the METMAN model. The model provides a representation of the suited environment during EVA. Incorporated in this representation is the outer suit environment. In this situation the outer suit environment consisted of the lab ambient metrics. Additionally, the added thermal sensor suite allowed for a higher accurate representation of the inner MK III suited environment during Lunar simulated EVA tasks. These higher accurate inputs allowed for better representation of suited operator thermal regulation and changes of metabolic activity. Corresponding outputs yielded simulated core temperature and mean skin temperature responses over time for various thermal loading. The simulated predictions of core temperature had shown to have general correlations for

accurate predictions, however for S1 the METMAN outputs did not respond quickly to temperature inflections (Figure 6.10 A). However, simulated predictions of S2 provided a more stable response to core temperature (Figure 6.11 A). The variability in the core temperature inflections during the R2 simulated EVAs could be attributed to the physiologic efficiency of the cardiovascular response to activity loads. The mean heart rate for suited operator S1 was significantly lower than that of suited operator S2 during rest and high metabolic loading (Table 6.1). The responses of quick increases and decreases of core temperature could be due to the efficiency of S1 expelling heat to the periphery. In the METMAN simulations the physiology of blood flow and cardiovascular changes is hard set to a general orientation that may not capture the variation of subject variability and cardiovascular fitness.

As a comparison to METMAN and to provide a quicker minute by minute determination of thermal loading, the similar technique of linear regressions was built for core temperature regressions. These regressions were built using heart rates, metabolic rates and suit thermal parameters. The predictions for S1 had shown to be comparable to the METMAN simulated core temperature and within 0.5 °C RMSE of original core temperature (Table 6.6). The thermal regression model for S1 had also shown a slight delay during quick decreases in core temperature (Figure 6.9 A). This factor for the regression model could be attributed to the use of only inlet LCG instead of the ΔLCG due to the S1 R1, attributed to technical error, to which the regression was built. Additionally, it was noted that during the S1 R1 simulated EVA the suit operator turned off the flow to the LCG at various times. However, from this regression model it was determined that the metric of MR/HR developed in Chapter 5 provided a good linear response incorporating both heart rate and metabolic rate components. This attributed to an added metric for multiple

regression terms and could provide a conversion factor if heart rate or metabolic rate instrumentation fails.

The thermal responses for S2 R2 was separated into two segments. This was due to a built-in break for the suited operator that had affected the core temperature values during this duration. For both segments the METMAN model predicted the total core temperature accurately with an RMSE output of 0.23 °C. As mentioned earlier the S2 suited operator had high heart rates that could be attributed with higher metabolic demand and less thermal efficiency. The core temperature in general for S2 R2 run did not have drastic inflection points but rather stayed constant in subtle slope changes at high core temperature values. During the S2 R2 regression predictions the core temperature had outperformed the METMAN modeling outputs. The regression for core temperature had term inputs for ΔLCG which added to that accuracy leading to a 0.12 °C RMSE. It was also noted that during the S2 R1 simulated EVA the suited operator did not turn off the LCG allowing for more consistent cooling and less inflections in the built regression model.

In addition to core temperature outputs the mean skin temperature was predicted using both the METMAN model and the regression techniques. The mean skin temperature regression model outperformed the METMAN model attributed to mean skin temperature. The METMAN model lagged the starting signal of mean skin temperature compared to both the original signal and the regression model. It could be attributed to heat transfer lags and heat storage thresholds within the model. The RMSE for both S1 and S2 predictions had shown to be relatively high with greater than 1 °C RMSE. The regression model showed slightly more accurate results during S1 predictions versus S2 predictions. This could be attributed to S1 turning off LCG flow at various times through out the R1 simulated EVA whereas S2 did not turn off LCG flow. The temperature

values then would result in higher range of mean skin temperatures in the regression for S1 leading to more accurate predictions during the R2 simulated EVA.

A basis for heat generation within the body has a dependency on workload and energy expenditure. As workload was shown to increase for the EVA task metabolic rates in turn increased as a result for both suit operators during both ARGOS simulations. As a correlated response cardiovascular metrics shown through also shifted with increasing and decreasing metabolic demand. It was found through the same techniques used in Chapter 3, HRV metrics could be used to view cardiovascular responses to increased energy expenditure. The main metrics in a flight environment that determined stress responses were that of frequency domain metrics LF, HF and LF/HF. In this study as metabolic demand increased LF/HF values also increased suggesting sympathetic dominance. As a corollary, it was also seen that LF values increased while HF values decreased also solidifying the observation of sympathetic response to increased energy expenditure and resultant increased workload. Further, short-term metrics of RMSSD and SDNN had shown to decrease with increased metabolic activity corresponding to increases in maximum and minimum heart rates as well as mean RR intervals.

Additionally, non-linear metrics corresponding to Poincare plot designators SD1 and SD2 show to have inverse shifts depicting interrelation of short-term and long-term autonomic responses to changing workloads. SD1 decreased more drastically with increased metabolic demand suggesting that with higher metabolic costing tasks short-term stress responses of the sympathetic nervous system increase. This is further seen when SD2 increases at those high metabolic tasks. Continually, Alpha-1 term for detrended fluctuation analysis shows decreased values of signal complexity at low metabolic loads while increasing in complexity for high metabolic demand. This further points to the short-term stress responses of sympathetic dominance

for increased workload. However, Alpha-2 term also does show decreased values at low workloads with slightly higher values for high metabolic tasks suggesting a connection to long-term stress responses. These HRV values show similar stress response in those seen in Chapter 3 with increased stress responses attributed to short-term HRV metrics. Pointing to the use of HRV to determine metabolic increased workload and increased stress responses on task.

6.6 Conclusions

In this chapter techniques were validated and further utilized to predict energy expenditure and thermal loading during simulated Lunar EVA in the MK III space suit. A thermal sensor suite was developed to gather suit operator core temperature and mean skin temperature while also gathering suit thermal data of liquid cooling garment temperature, suit temperature and suit humidity changes. The thermal data in tandem with cardiovascular metrics and metabolic rates were used to develop linear regression models to predict thermal loading. Techniques of metabolic prediction using heart rates were used from Chapter 5 to build upon improved prediction models for suited training. These same techniques were used to develop a cardiothermal regression model to predict core temperature and mean skin temperature of the suit operator during training scenarios. The regression models were comparable to outputs from a popular human thermal regulation model METMAN and at times outperforming predictions of mean skin temperature. Additionally, HRV metrics identified from Chapter 3 were used to further define high metabolic demanding tasks corresponding to increased sympathetic dominance and short-term stress responses. Ultimately, these techniques can further space suit development by adding elements of predictive human performance for improved training scenarios during simulated gravity EVA.

References

[87] J. R. Braden and D. L. Akin, "Development and Testing of a Space Suit Analogue for Neutral Buoyancy EVA Research," Jul. 2002, pp. 2002-01–2364. doi: 10.4271/2002-01-2364.

[88] I. L. Schlacht *et al.*, "Space Analog Survey: Review of Existing and New Proposal of Space Habitats with Earth Applications," Jul. 2016, Accessed: Aug. 02, 2019. [Online]. Available: https://ttu-ir.tdl.org/handle/2346/67692

[171] D. E. Watenpaugh, "Analogs of microgravity: head-down tilt and water immersion," *Journal of Applied Physiology*, vol. 120, no. 8, pp. 904–914, Feb. 2016, doi: 10.1152/japplphysiol.00986.2015.

[207] M. Wuligoru, R. Huwkins, G. F. Humbert, and L. H. KEcznetz, "APOLLO EXPERIENCE REPORT - ASSESSMENT OF METABOLIC EXPENDITURES," *Tech Rep NASA TN D-7883*, 1975.

[214] M. Reagan, B. Janoiko, J. Johnson, S. Chappell, Ph.D., and A. Abercromby, "NASA's Analog Missions: Driving Exploration Through Innovative Testing," presented at the AIAA SPACE 2012 Conference & Exposition, Pasadena, California, Sep. 2012. doi: 10.2514/6.2012-5238.

[215] D. Eppler, "Desert Research and Technology Studies (DRATS) 2010 Science Operations: Operational Approaches and Lessons Learned for Managing Science during Human Planetary Surface Missions," *Acta Astronautica*, pp. 224–241, Mar. 2012.

[216] O. S. Bekdash *et al.*, "Development and Evaluation of the Active Response Gravity Offload System as a Lunar and Martian EVA Simulation Environment," p. 12.

[217] A. F. J. Abercromby *et al.*, "Crew Health and Performance Extravehicular Activity Roadmap: 2020," p. 74, 2020.

[218] D. C. E. Larsen, "NASA Experience with Pogo in Human Spaceflight Vehicles," p. 23.

[219] J. Norcross *et al.*, "Characterization of Partial-Gravity Analog Environments for Extravehicular Activity Suit Testing," *NASA/TM-2010-216139*, Dec. 2010.

[220] J. Norcross, S. Chappell, and M. Gernhardt, "Lessons Learned from Performance Testing of Humans in Spacesuits in Simulated Reduced Gravity," NASA Technical Report, NASA/TP-2010-00005154, 2010.

[221] J. Norcross, S. Jarvis, O. Bekdash, S. Cupples, and A. Andrew, "EVA Human Health and Performance Benchmarking Study Overview and Development of a Microgravity Protocol," NASA Technical Report, NASA/TP-2017-0000796, 2017.

[222] P. Valle, "Reduced Gravity Testing of Robots (and Humans) Using the Active Response Gravity Offload System," NASA technical Report, NASA/TP-2017-0008856, 2017.

[223] C. R. Cullinane, R. A. Rhodes, and L. A. Stirling, "Mobility and Agility During Locomotion in the Mark III Space Suit," *Aerospace Medicine and Human Performance*, vol. 88, no. 6, pp. 589–596, Jun. 2017, doi: 10.3357/AMHP.4650.2017.

[224] F. A. Korona, J. Norcross, B. Conger, and M. Navarro, *Carbon Dioxide Washout Testing Using Various Inlet Vent Configurations in the Mark-III Space Suit*. 44th International Conference on Environmental Systems, 2014. Accessed: Oct. 24, 2021. [Online]. Available: https://ttu-ir.tdl.org/handle/2346/59676

[225] A. Abercromby, S. S. Thaxton, E. A. Onady, and S. L. Rajulu, "Reach Envelope and Field of Vision Quantification in Mark III Space Suit using Delaunay Triangulation," *NASA/TP-2006-213729*, Jan. 2006.